PCCP

Accepted Manuscript

ROYAL SOCIETY OF CHEMISTRY

www.rsc.org/pccp

Elucidating the Role of Copper as Redox Additive and Dopant on the Performance of PANI based Supercapacitor

Kavita Pandey, Pankaj Yadav, Indrajit Mukhopadhyay[*]

School of Solar Energy, Pandit Deendayal Petroleum University, Gandhinagar- 382007, Gujarat, India

ABSTRACT

In this article, the role of copper (Cu) as a redox additive and dopant on the performance of Polyaniline (PANI) based supercapacitor was thoroughly investigated. The electrochemical properties of PANI in H_2SO_4, H_2SO_4+$CuSO_4$ and Cu doped PANI in H_2SO_4 were studied using Cyclic Voltammetry (CV) and Impedance Spectroscopy (IS). The CV result indicates that the capacity of PANI in H_2SO_4 was significantly improved with the introduction of Cu^{2+} ions to the electrolyte; yet appearing unstable because of under potential deposition of copper over PANI surface and relatively irreversible nature of redox reaction. However, a stable and improved performance was obtained for Cu doped PANI due to the combined effect of an increase in conductivity and the surface modification of PANI film. For Cu doped PANI, nearly ~2.4 and ~1.5 fold improved interfacial capacitance was achieved than that of PANI (H_2SO_4) and PANI (H_2SO_4+$CuSO_4$) respectively. The obtained Nyquist spectra for all the configurations was analysed using an equivalent circuit to understand the fundamentals of capacitive and resistive response of the supercapacitor. The IS measurement leads to direct determination of parameter like series resistance, rate capability of electrode, ion diffusion phenomena and interfacial capacitance. The experimental results and their analysis will have

significant impact on understanding the role of doping and redox additive on the performance of PANI based supercapacitor and also lay the basis to design a supercapacitor with appropriate electrode and electrolyte material for numerous industrial and consumer applications.

1. INTRODUCTION

Supercapacitors have been regarded as one of the most promising source for automotive and portable system applications due to high power density, fast charge discharge rate and long life cycle.[1] A wide range of metal oxides (Ni, Fe, In, Co, Ru, Mn etc.), conducting polymer (Polyaniline, Polypyrrole, etc.) and carbonaceous material (Graphene, Single wall carbon nanotubes, Multi wall carbon nanotubes, etc.) are used for supercapacitor application.[2-6] The enhanced redox capability of conducting polymer and metal oxide makes it more suitable for redox capacitors (or pseudocapacitors) application while the charge storage capability of carbonaceous materials at electrode-electrolyte interface makes it a suitable candidate for electrochemical double layer capacitor (EDLC) application. In general, the commercial available EDLCs are made of electrically conductive activated carbons with a specific capacitance in the range of 80-110 Fg^{-1} (40-70 Fcm^{-3}) for organic electrolytes and 100-160 Fg^{-1} (40-70 Fcm^{-3}) for aqueous electrolytes.[7] For pseudocapacitor application, Polyaniline (PANI), a conducting polymer is a material of great interest because of its environmental stability, low cost, easy doping-dedoping, a good reversibility and electro activity.[8,9] The metal oxides of Ru and Mn are also widely employed for pseudocapacitor application. Zheng et al.[5] has employed the hydrous form of ruthenium oxide for electrochemical capacitors. Lee et al.[6] have demonstrated a capacitance of 700 Fg^{-1} and 200 Fg^{-1} for amorphous, hydrated RuO_2 and MnO_2 electrodes respectively. The synthesis of PANI with various carbonaceous material and metal oxides to develop an economical electrode material with higher capacity is of great interest. Chen et al.[10] obtained a remarkable energy density of 84 $Whkg^{-1}$ for PANI

nanotube grown by utilizing MnO_2 templates. Maser et al.[11] demonstrated an order of magnitude increase in the electrical conductivity of carbon nanotube-PANI composite as compared to pure PANI. Tai et al.[12] fabricated a 3D graphene-PANI composite hydrogel via a self-assembled method which showed a supercapacitive performance of 334 Fg^{-1}. Mi et al.[13] synthesized nano fiber structured PANI electrode for supercapacitor application, which shows a specific capacitance of 428 Fg^{-1} in H_2SO_4 electrolyte. Meng et al.[14] demonstrated a novel method to prepare paper like CNT/PANI composites which showed a superior electrochemical performance such as higher specific capacitance, lower internal resistivity, and more stability under different current loads.

The capacitive performance of supercapacitor is also being improved by doping the electrode material with different kind of transition metal or by adding redox active species into the electrolyte. The concept of doping was first introduced for Iridium doped PANI by Hu et al.[15] for electrochemical capacitors application. They have also showed an enhancement in stability, high power performance and electrochemical reversibility of redox reactions by adding Platinum nanoparticles in PANI matrix.[16] Khan et al.[17] has proposed that PANI doped with CuO results in the growth of nanofiber like morphology with high conductivity. Xu et al.[18] has polymerized PANI with Cu^{2+} ion and used it as an electrode material in supercapacitor which demonstrate a specific capacity of 618 Fg^{-1}. Dhibar et al.[19] has polymerize PANI with different doping levels of $CuCl_2$ which showed a higher specific capacitance and better thermal stability of PANI in doped form. The use of redox active sources (hydroquinone, KI, $CuSO_4$ and so on) with conventional electrolytes (H_2SO_4, KOH, KCl, etc.) is directly involved in the electron transfer redox reaction where the capacitance is enhanced due to surface pseudo capacitive contribution at electrode-electrolyte interface. Li et al.[20] have obtained a specific capacity of 223 $mAhg^{-1}$ for redox mediator Fe^{2+} and Cu^{2+} added H_2SO_4 electrolyte. Very recently, Qian et al.[21] has studied CuS nanotubes in redox

active polyelectrolyte (0.5M NaOH/ 0.5M Na_2SO_4/ 0.5M S powder) and obtained a specific capacitance of 2393 Fg^{-1} at 10 mVs^{-1} with an energy density of 592 $Whkg^{-1}$ at 15 Ag^{-1}. Chen et al.[22] reported a specific capacitance of 553 Fg^{-1} and 288 Fg^{-1} in hydroquinone added H_2SO_4 and 1M H_2SO_4 electrolyte, respectively for PANI-graphene composite.

Recently, some primary work has been reported on the performance of Cu doped PANI by varying the doping level. However, in literature there is scarcity of reports available for defining the role of transition metal as a dopant or redox additive which is essential for designing a high power/ high energy supercapacitor. In the present work, the electrochemical characteristics and pseudo capacitive effect of Cu^{2+} as a redox additive in electrolyte or dopant in PANI nanostructure have been investigated. Under the configuration of PANI in 1M H_2SO_4, PANI in 1M H_2SO_4+ 0.5M $CuSO_4$ and Cu doped PANI in 1M H_2SO_4, the present study is mainly focused on (i) to elucidate the role of Cu^{2+} as redox additive and dopant on the performance of supercapacitor, (ii) the influence of redox active electrolyte and doping on the charge transfer phenomenon at electrode-electrolyte interface and (iii) complex frequency analysis of supercapacitor which is necessary for practical applications. Herein it is observed that $CuSO_4$ as a redox additive offers a higher energy storage with low power delivering rate while PANI in H_2SO_4 offers a lower capacitance with high power delivering rate. Interestingly, the Cu doped PANI nanostructure enhances both the energy storage and capacitance retention. Moreover, the obtained result proposes that Cu doped PANI have a promise for devising as a high performance electrochemical capacitor.

2. Experimental Section

Preparation and Characterization of electrodes. The PANI electrodes were prepared from the aniline solution as follows. The monomer solution of aniline purified by double distillation and stored in a nitrogen glove box was prepared in MilliQ water using analytical

grade hydrochloric acid (HCl). The electropolymerization were conducted in a one compartment three electrode cell containing a mixture of 2% aniline in 1M aqueous HCl at room temperature. A fluorine doped glass substrate having a sheet resistance of ~12Ω/□ is used as a working electrode with Ag/AgCl and Pt ring as a reference and counter electrode respectively. The fluorine doped glass substrate was ultrasonically washed with acetone, ethanol and distilled water each for 15 minutes respectively. The cell and counter electrodes were cleaned with freshly prepared 1:1 H_2O_2/H_2SO_4 solution followed by ultrasonication in MilliQ water. The same electropolymerization method was employed to deposit copper doped PANI film from the monomer solution containing a mixture of 2% aniline in 1M HCl and 0.5M $CuSO_4.5H_2O$. After each deposition, the remaining electrolyte was soaked from the electrode surface with filter paper and kept for drying.

The surface morphology of all the samples was collected using Carl Zeiss scanning electron microscope under ultrahigh vacuum conditions. The samples were placed onto circular adhesive carbon films to be affixed to Aluminium sample stubs. The FTIR spectra were recorded with Nikolet 6700. The Raman spectra and XPS are employed to understand the chemical difference between PANI and Cu-PANI.

Electrochemical Studies of electrodes. The electrochemical properties of electrode in three different configurations were studied by Cyclic Voltammetry (CV) and Electrochemical Impedance Spectroscopy (EIS) using Ag/AgCl (saturated KCl) and Pt ring as a reference and counter electrode respectively. PANI as a working electrode was examined in 1M H_2SO_4 and 1M H_2SO_4 mixed with 0.5M $CuSO_4$ redox active electrolyte which will be further referred as PANI (H_2SO_4) and PANI (H_2SO_4+$CuSO_4$) respectively, in the article. To study the effect of doping on the supercapacitive properties, the Cu doped PANI electrode was examined in 1M H_2SO_4, referred as Cu-PANI (H_2SO_4) hereafter. The electrochemical properties of all the configurations were studied through CV within the potential window of 0 to 0.7V at different

scan rates. Moreover, the cycle life of the electrode was tested for 1000 cycles. EIS was carried out at an open circuit potential (OCP) and at different applied potential by applying a perturbation signal of 10 mV amplitude in the frequency range of 0.1 Hz to 100 kHz. Only after the OCP of the system was stabilized, the electrochemical measurements were carried out at room temperature by using CH Instrument 660D potentiostat equipped with a general purpose electrochemical system software. The interfacial capacitance of the electrodes was calculated by using Eq. (1)

$$C = \frac{I\Delta t}{A\Delta V} \quad (1)$$

Where, I is the discharge current, A is the area of electrode, Δt is the discharge time and ΔV is the potential range. The real part (C') of the complex capacitance can be extracted from the impedance data according to Eq. (2),

$$C'(\omega) = \frac{-Z''(\omega)}{\omega|Z(\omega)|^2} \quad (2)$$

Where, $Z''(\omega)$ is the imaginary part of complex impedance $Z(\omega)$ and ω is the angular frequency. The value of $C'(\omega)$ obtained at low frequency can be used as the static capacitance of the electrode.[23]

3. Results and Discussion

Optical Analysis. Fig. 1A depicts the FTIR spectra of PANI and Cu-PANI. The obtained spectra for both the electrodes are essentially the same with some peak shifting indicating the dominance of chain protonation reaction. The common peaks situated at 790, 1130, 1220, 1265 and 1640 cm^{-1} for both the electrodes is attributed to the following vibrations: out of plane bending vibration of C-H in benzene ring π disubstituted, C-H bending of the quinoid ring, stretching vibration of the $CN^{\bullet+}$ in the polaron structure of PANI, stretching of C-N

secondary aromatic amine and stretching vibration of C=N respectively.[24] The red shift of the two absorption peaks from 1568 to 1562 cm^{-1} and 1475 to 1457 cm^{-1} in Cu-PANI is referred to be a signature of the conversion of quinoid rings to benzenoid rings by proton induced spin unpairing mechanism.[24] This mechanism is considered to be an indication of the increase in degree of charge delocalization on the PANI backbone due to protonation.[25]

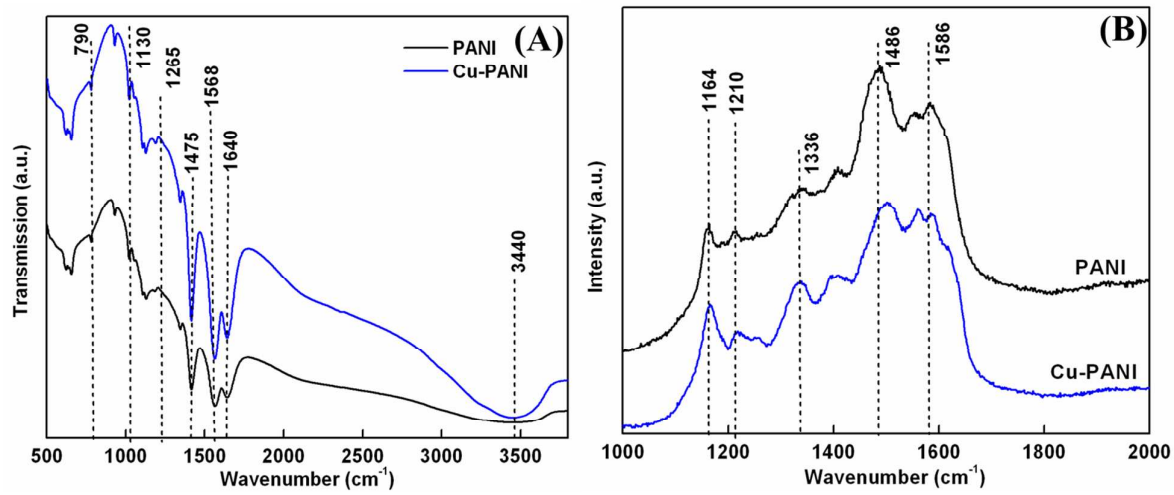

Fig. 1 (A) FTIR and (B) Raman spectra of PANI and Cu-PANI electrodes

The Raman spectra of PANI and Cu-PANI at 1064 nm excitation signal are shown in Fig. 1B. For PANI, the peaks observed at 1164, 1210, 1486 and 1586 cm^{-1} corresponds to the C-H bending of quinoid ring, C-H bending of the benzenoid ring, C=C stretching of the quinoid ring and stretching of benzenoid ring respectively.[24] As compared to the spectra of pure PANI, the $C\text{-}N^{\bullet+}$ stretching peak gradually shifts to the higher wavenumber from 1341 to 1394 cm^{-1}. Also, the most characteristic Raman band of the radical cation is observed at 1336 cm^{-1} for Cu-PANI. This typical band is expected when the quinoid rings are converted to benzenoid rings. A similar conclusion for Cu-PANI is drawn from the FTIR analysis. Another change is the 1486 cm^{-1} band assigned to the stretching of the quinoid di-imine units

diminishing in Cu-PANI, which indicates the decrease in the amount of quinoid units in the polymer chain due to the doping process.[26]

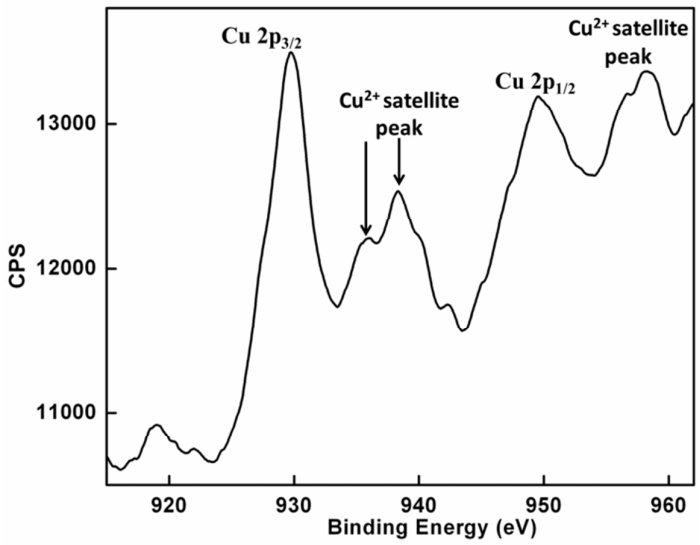

Fig. 2 Copper 2p XPS spectra of Cu-PANI film

PANI and Cu-PANI films were subjected to XPS examination for the confirmation of formation of Cu^{+} within the Cu-PANI matrix. The C 1s core level spectra for PANI and Cu-PANI are given in Fig. S1 of ESI†. The Cu 2p core level spectra for Cu-PANI is shown in Fig. 2. The C 1s spectrum for both the electrodes exhibits an asymmetric characteristic indicating the presence of structural defects.[27] The four peaks deconvoluted by Gaussian fitting centered at 284.1, 285.08, 285.8 and 286.6 eV belongs to C-C or C-H, C-N or C=N, C-N^{+} or C=N^{+} and C=O or C-O respectively for both the films. The C=O/C-O functional groups observed for both the electrodes are attributed to the presence of BQ and HQ type degradation product. The presence of Cu $2p_{3/2}$ (Fig. 2) peak centered at 933.6 eV along with the presence of small satellite peak is assigned to Cu (II). The major Cu $2p_{3/2}$ peak centered at 932.5 eV is assigned to Cu (I). Both the observed peaks at 933.6 eV and 932.5 eV for Cu-PANI is consistent with the previous reports.[18]

Morphological Analysis. The surface morphology of PANI and Cu-PANI was studied using SEM as shown in Fig. 3A and 3B respectively. The electrochemically synthesized PANI has fibrillar like morphology aligned parallel to the plane of fluorine doped glass substrate while maintaining the random orientation within the plane. The Cu doped PANI (Fig. 3B) also appears to have fibrillar morphology with a smaller diameter of PANI Nanorods. The SEM study reveals that the average Nanorod diameter of PANI and Cu doped PANI is ~461 nm and ~142 nm respectively. Transition metal salts like Cu were found to be able to interact with PANI chains directly and induces a morphological change in PANI films. The difference in the morphology of PANI and Cu-PANI is most likely to be derived from a change in coordination geometry of metal ion i.e. Cu^{2+}.[28] Cu^{2+} ion has a coordination number less than or equal to 6 with tetrahedral coordination geometry. Thus, one Cu^{2+} ion may bind with more than one nitrogen sites of PANI chain or form a inter chain linkage among several adjacent PANI chains by coordination. Both intra and inter chain connections may lead to a more coil like conformational change or a more twisted aggregation of PANI chains and thus a lower nanorod dimension in Cu-PANI.[28] Also, the change of counterion i.e. SO_4^{2-} in $CuSO_4$ affects the regime of doping and thus the morphology.

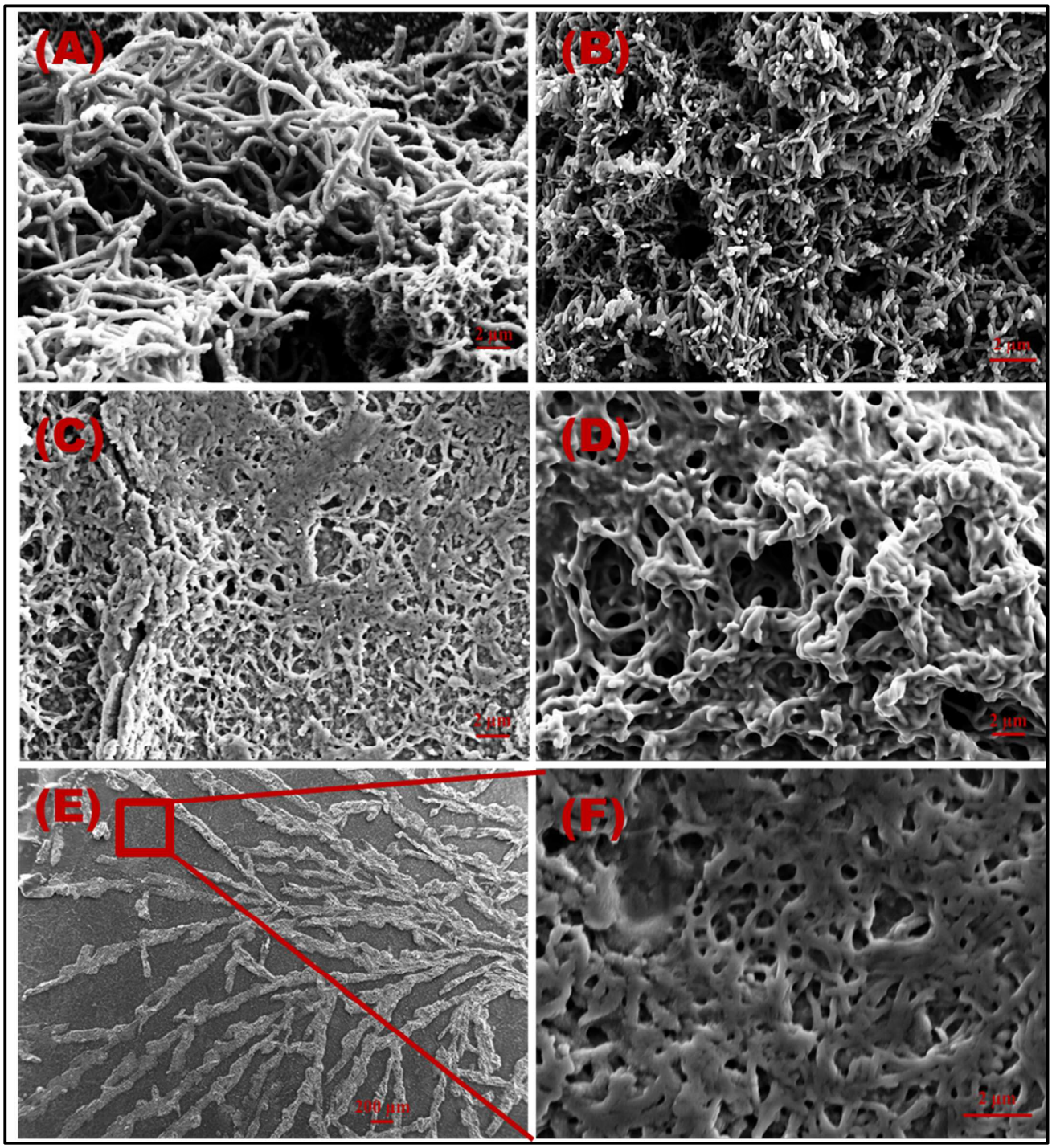

Fig. 3 SEM images of (A) as-deposited PANI (B) Cu doped PANI (C) PANI (H_2SO_4) after cycling for 400 cycles (D) Cu-PANI (H_2SO_4) after cycling for 400 cycles (E) PANI (H_2SO_4+$CuSO_4$) after cycling for 400 cycles (F) High magnification image of the squared area

To examine the influence of redox additive and dopant on the reaction mechanism of Cu^{2+} and PANI, the surface morphology of PANI (H_2SO_4) Cu-PANI (H_2SO_4) and PANI (H_2SO_4+$CuSO_4$) after being subjected to 400 cyclic tests are analysed using SEM (Fig. 3C, 3D and 3E respectively).

The doping and de-doping of H^+ ions into or from the PANI and Cu-PANI chain results in the swelling and shrinkage of the nanostructured conducting polymer. The cycling of PANI in 1M H_2SO_4 + 0.5M $CuSO_4$ results in the electrodeposition of Cu fractals on the surface of PANI (Fig. 3E). The deposition and dissolution of Cu on FTO substrate in $CuSO_4$ + H_2SO_4 electrolyte has been studied independently and shown in Fig. S2 of ESI†. High magnification image of the squared area (Fig. 3F) clearly shows that the PANI Nanorod gets swelled during cycling that may result in the lower effective surface area and interfacial capacitance. To confirm these results, the DC (Cyclic Voltammetry) and AC (Electrochemical Impedance Spectroscopy) responses of all the configurations is the subject of discussion in the further section.

DC Voltage dependent Cyclic Voltammetry. The electrochemical property of PANI (H_2SO_4), PANI (H_2SO_4+$CuSO_4$) and Cu-PANI (H_2SO_4) were examined through Cyclic Voltammetry (CV) and Electrochemical Impedance Spectroscopy (EIS) measurements. The CV response of Cu doped PANI and PANI film in different electrolytes within an optimized voltage window of 0 to 0.7 V vs. Ag/AgCl reveals an ion PANI interaction, impact of pore structure & ion size on the adsorption of ion within PANI matrix, and the transport phenomena. Fig. 4A shows the representative CV behaviour of PANI (1M H_2SO_4), PANI (1M H_2SO_4+ 0.5M $CuSO_4$) and Cu-PANI (1M H_2SO_4) in three electrode configuration at a sweep rate of 5 mV/s. The electrochemical response current of all the configurations shows that the positive sweep is nearly asymmetric to their corresponding counter part of negative sweep with reference to zero current line. A predominant characteristic peak during the

positive and negative sweep is usually the evidence of pseudo capacitive behaviour and corroborates the presence of Faradaic current. A pair of redox peak at potentials negative to 0.3 V is attributed to the redox transition of PANI between leucoemeraldine (semi conductive state) and a polaronic emeraldine form (conductive state). The redox peak at potentials above 0.65 V is attributed to the formation/reduction of bipolaronic pernigraniline and its resonance form, i.e. protonated quinonediimine.[29-31] A constant current during the positive and negative sweep in the bias range (~ 0.35 V to 0.7 V) resembles the rectangular shape of nearly ideal capacitor with a small internal resistor. The CV response of PANI in all the configuration, at different sweep rate, follows the description of $i = i_r + \upsilon_{dc} C_i$, where i represents the net current, i_r, υ_{dc} and C_i represents the Faradaic current, scan rate and scaled value of interfacial capacitance respectively.[32] The voltammetric currents at potentials positive to 0.2 V are linearly proportional to the scan rate of CV (ESI†).[30] To have an insight of linear equation $(i = i_r + \upsilon_{dc} C_i)$, a scaled version of obtained data (Fig. 4A) for PANI (H_2SO_4), PANI (H_2SO_4+$CuSO_4$) and Cu-PANI (H_2SO_4) is shown in Fig. 4B, 4C and 4D respectively. Increasing the sweep rate from 5 to 50 mV/s for PANI (H_2SO_4) affects both the regions i.e. transient region where current direction is abruptly inversed and interfacial capacitance region (after transient period). The change in transient region with the increase in sweep rate signifies that a high ionic flux within the porous PANI network is necessitated. However, after this transient period, the interfacial capacitance in the bias range of 0.35 V to 0.62 V was nearly unaffected by increasing the sweep rate (Fig. 4B), suggesting that the accessibility of PANI pores by electrolyte ions was not obstructed from reaching the inner surface area even at such high sweep rates. Also, the interfacial capacitance in the bias range of 0.15 V to 0.35 V gradually reduces on both the sides of zero current axis with sweep rate attributing to the presence of inner active sites which cannot precede the redox transition completely. The predominant oxidative and reductive peak shifts negatively and positively (change in ΔE_P)

simultaneously with the scan rate. The change in ΔE_P with the scan rate results from kinetic effects and uncompensated ohmic drop.[33] A change of 0.132 V is observed for PANI film in H_2SO_4 electrolyte with the change in scan rate from 5 to 50 mV/s.

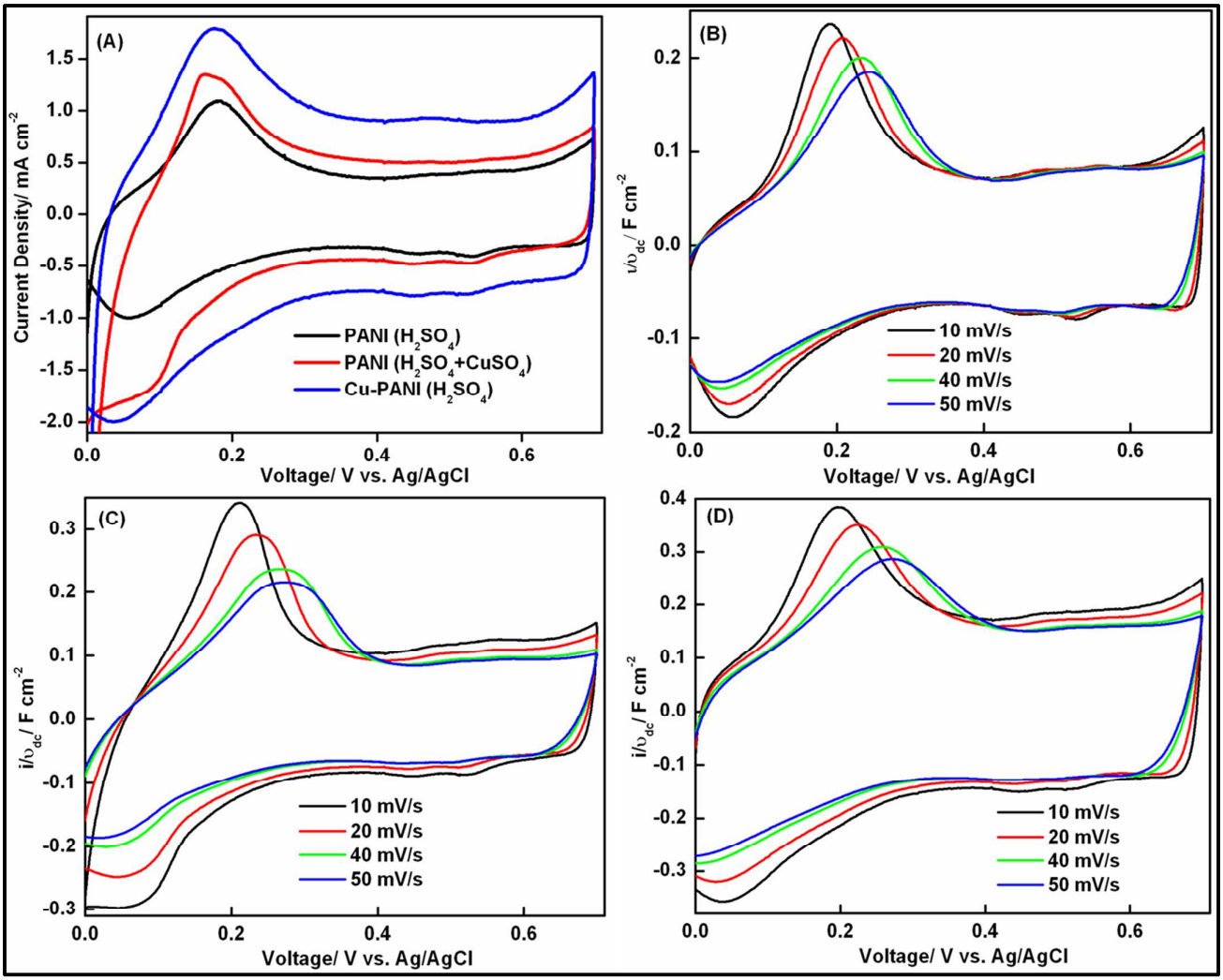

Fig. 4 Electrochemical characterization in a three electrode cell: (A) cyclic voltammetry of different configuration at 5mV/s, Effect of sweep rate on cyclic voltammogram for (B) PANI (H_2SO_4), (C) PANI (H_2SO_4+$CuSO_4$) and (D) Cu-PANI (H_2SO_4).

Interestingly, a markable change is observed in the CV curves of PANI film while switching the electrolyte from H_2SO_4 to H_2SO_4 + $CuSO_4$ solution, which can be mainly attributed to the following reasons: First, a higher current is observed for PANI in Cu^{2+} loaded H_2SO_4

electrolyte than PANI (H_2SO_4) at all the bias range probed here, which can be considered to be a combination of the following two parts i.e. a) A higher amount of positive ion (H^+, Cu^+) necessitates the pores of PANI and take part in pseudo Faradaic reaction and b) The process of progressive occupation of electrode surface sites by underpotential deposited Cu species also contribute to the pseudo capacitance. The explained mechanism becomes more prominent by observing the SEM image of PANI in H_2SO_4+$CuSO_4$ electrolyte in Fig. 3E, where Cu fractals are grown over PANI nanorod surface. A similar result for carbon electrode in H_2SO_4 + $CuSO_4$ electrolyte is observed by other authors.[20] A general accepted mechanism for electrodeposition and dissolution of Cu in sulphate solution is given by Li et al.[20] and Kumar et al.[34] through two consecutive step as follows:

$$Cu^{2+}{}_{(aq.)} + e^- \rightleftarrows Cu^+{}_{(adsorb)}$$

$$Cu^+{}_{(adsorb)} + e^- \rightleftarrows Cu_{(deposit)}$$

Second, a higher rate of change in transition region with the sweep rate is observed for PANI (H_2SO_4+$CuSO_4$) as compared to PANI (H_2SO_4). The higher rate of change suggests that a greater resistance is faced by electrolyte ions travelling within the polymer matrix. The interfacial capacitance of PANI (H_2SO_4+$CuSO_4$) decreases at a faster rate than PANI (H_2SO_4) at higher sweep rate. Since the size of H^+ ion in both the solvated and desolvated state is smaller than Cu^{2+} ion; it is expected that ionic accessibility of internal micropores of PANI by H^+ ion is negligibly affected as compared to Cu^{2+} ion. Also, the electrodeposited Cu fractals on PANI surface during the electrochemical measurement restrict the ion accessibility of PANI by effectively reducing the total surface area. A similar result for sulphur activated carbon in different aqueous electrolytes i.e. LiCl and HCl has been obtained by other researcher.[35] The decrease in capacitance at a higher sweep rate also suggests that the electrochemical redox reaction between Cu^{2+} ions in liquid state and deposited copper

(solid state) are not fully reversible and the deposited copper being only partly, as opposed to wholly, desorbed and re-oxidised to Cu^{2+} during the positive/negative cycles.[20,36] A higher peak potential ΔE_P obtained for $H_2SO_4 + CuSO_4$ electrolyte than that of H_2SO_4 signifies the higher intrinsic ohmic losses. Moreover the CV plot of PANI ($H_2SO_4 + CuSO_4$) exhibits a higher slope (higher current at higher voltage) than that of PANI (H_2SO_4), indicating a significant higher leakage current for redox additive electrolyte. From the above discussion it can be inferred that the decrease in capacitance in the transition region & pseudo region at higher sweep rate for PANI ($H_2SO_4 + CuSO_4$) is mainly related to the higher resistance faced by the electrolyte ions while traveling within the PANI matrix and a slower pseudo capacitive redox reaction between electrodeposited Cu fractals and electrolyte ions.

In order to assess the effect of Cu doping in PANI matrix on the electrochemical performance, the CV graphs of Cu-PANI (H_2SO_4), PANI (H_2SO_4+ $CuSO_4$) and Cu-PANI (H_2SO_4) in Fig. 4 are compared. The CV plot of Cu-PANI (H_2SO_4) changed markedly as compared to the other two configurations. First, a higher Faradaic feature is observed for Cu doped PANI than the PANI electrode. The Faradaic current at electrode – electrolyte interface is mainly influenced by the presence of active sites at electrode, ion mobility and easy insertion – desertion of electrolyte ions in the polymer matrix. A higher Faradaic feature of Cu doped PANI is apparent from the following morphological and interfacial features i.e. (a) A comparatively smaller Nanorods with widely homogenous distribution of PANI film offers a higher surface area at electrode electrolyte interface which provides a shorter path length for electron and ion transport and (b) During Cu doping through polymerization, Cu^{2+} ion are reduced to Cu^{+} and aniline is oxidised to PANI. The Cu ions act as a redox active catalyst and improves the delocalization of π electrons through the enhance interactions between Cu ions and π electron density of polymer chain.[18,37]

Second, the existence of Cu^{2+} in PANI matrix shifts the oxidation-reduction peaks, and also affects its operating voltage range and reversibility. In general, due to the consideration of electronic conductivity, electrochemical reversibility and stability the optimized potential window for PANI based electrode is in between 0.2 to 0.7 V.[30,38] Due to the narrow potential window between 0.2 to 0.7 V vs. Ag/AgCl, the electrochemical energy stored in a supercapacitor is limited as $E = {C(\Delta V)^2}/{4}$ where ΔV is the working potential window. In this scenario, the doping of Cu^{2+} in PANI matrix can effectively improve the energy storage capability of PANI electrode by improving both, C and ΔV. In this article, for comparison of different configurations a common mechanistic in terms of operating potential window 0 to 0.7 V is used.

Third, the rate of change in transient region for Cu-PANI (H_2SO_4) and PANI (H_2SO_4+ $CuSO_4$) with the increase in sweep rate is almost same. The interfacial capacitance in the bias range (0.35 V to 0.62 V) for Cu-PANI (H_2SO_4) and PANI (H_2SO_4+ $CuSO_4$) is affected with the change in sweep rate while an independent behaviour of interfacial capacitance with sweep rate is observed for PANI (H_2SO_4). It shall be noted here that such a capacitance is mainly associated with the redox reaction of PANI,[29] where the metallic Cu ions in Cu-PANI (H_2SO_4) and PANI (H_2SO_4+ $CuSO_4$) have a favourable pseudo capacitive effect. Also, a same rate of change in interfacial capacitance in the bias range of 0.15 V to 0.35 V is observed for Cu-PANI (H_2SO_4) and PANI (H_2SO_4).

The Ragone plots (Fig. 5A) obtained from the discharge curves of all the configurations provides information about the available power and the optimum working region of a storage device. A maximum specific energy with a higher specific power is obtained for Cu-PANI (H_2SO_4) as compared to the other configurations. The higher value of specific energy for Cu-PANI (H_2SO_4) is due to the higher specific capacitance and higher working cell voltage. The

obtained value of specific energy and power for Cu-PANI is comparable to the previously reported results by other authors.[18] The factors such as discharge current, internal resistance and temperature affect the coulomb and energy efficiency. The coulomb efficiency of PANI (H_2SO_4), PANI (H_2SO_4+$CuSO_4$) and Cu-PANI (H_2SO_4) at a scan rate of 10 mVs^{-1} is 86.3%, 84.1% and 78.7% respectively. The energy efficiency of PANI (H_2SO_4), PANI (H_2SO_4+$CuSO_4$) and Cu-PANI (H_2SO_4) at a scan rate of 10 mVs^{-1} is 76.8%, 75.3% and 70.8% respectively. Based on the potential window of CV curves (Fig. 4), the electrical energy charged and delivered from the electrode is equal to the area under the charging and discharging curve respectively, where the difference between the charge and discharge energies represent the energy loss in a storage device. The energy losses for PANI (H_2SO_4), PANI (H_2SO_4+$CuSO_4$) and Cu-PANI (H_2SO_4) are approximately in the range of 7-11%. Such a significant energy loss not only reduces the capacitive performance but also increase the cell temperature to an unacceptable level, especially under the repeated operation.[39] Fig. 5B shows the interfacial capacitance as a function of cycle number for all the configurations. The Cu-PANI (H_2SO_4) exhibits the highest retention ratio of 54% as compared to 33% and 42% of PANI (H_2SO_4+$CuSO_4$) and PANI (H_2SO_4), respectively. The retention ratio for Cu-PANI (H_2SO_4) is comparable to the previously reported results by other authors for similar configuration.[18]

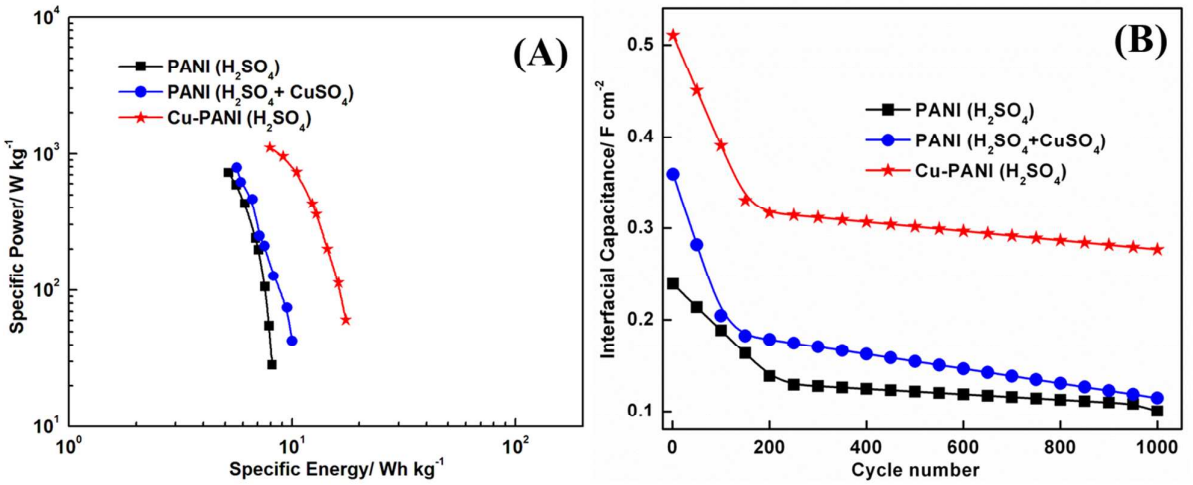

Fig. 5 (A) Ragone plot and (B) variation of interfacial capacitance as a function of cycle number for all the configurations

Electrochemical Impedance Spectroscopy. The analysis of cyclic voltammogram reveals that Cu-PANI (H_2SO_4) exhibits a comparatively higher pseudo capacitance. Whereas PANI surface physisorption in H_2SO_4+$CuSO_4$ (redox additive) electrolyte reveals a higher pseudo capacitance with low capacity retention as compared to PANI (H_2SO_4). The effect of these observed phenomena on the values of resistance and capacitance of supercapacitor can be further explained by Electrochemical Impedance Spectroscopy (EIS). EIS is a frequency domain technique that can reveal the complex phenomena of electron interception and diffusion at electrode-electrolyte interface.[40] The principle objective of EIS measurement is to gain an insight into the influence of doping and redox additive electrolyte on the resistive and capacitive element of supercapacitor.

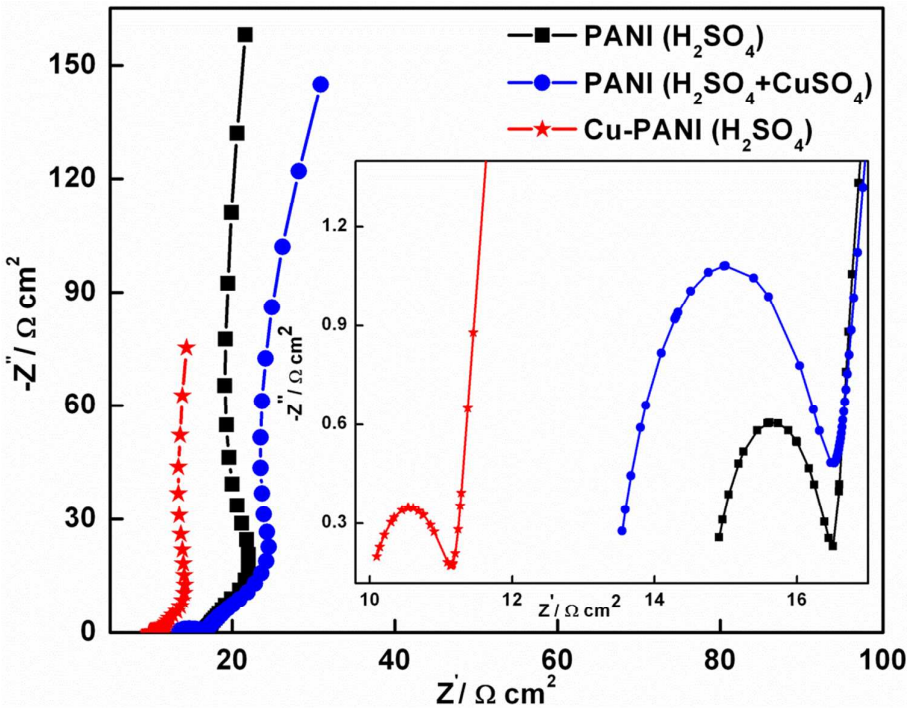

Fig. 6 Nyquist plot of the different configurations at open circuit potential. The inset shows the higher frequency details of the impedance spectra.

The EIS spectra obtained for all the configurations as a function of applied potential is shown in ESI†. The left most point of the EIS spectra represent the maximum frequency (100 kHz) while the right most point represents the minimum frequency (0.1 Hz). The obtained Nyquist spectra for all the configurations consists of a linear line in the low frequency region followed by a constant phase element typified by Warburg element and a semicircle in the high frequency region. From the obtained EIS curve and our previous study[8], a reasonable equivalent circuit (ESI†) is proposed to fit the experimental data. The semicircle in the high frequency region is modelled by a parallel combination of Faradaic leakage resistance (R_F) and the double layer capacitance (C_{dl}). The intersection point of the Nyquist spectra at high frequency with the real axis is represented by series resistance R_s.[41] The Nyquist spectra in the mid frequency region pertains to the diffusion of ions into the bulk of electrode and is represented by Warburg element W_0. The Warburg element, W_0 is expressed as $A/(j\omega)^m$,

where A is called the Warburg coefficient, ω is the angular frequency and m is an exponent. At a very low frequency a straight line parallel to the imaginary axis, inclined at an angle to real axis, is modelled through parallel combination of polarizable interfacial capacitance (C_i) and diffusion resistance (R_d). The expression for the impedance response of CPE is given by Eq. (3),

$$Z(CPE) = \frac{1}{Y_0(j\omega)^n} = \frac{1}{Y_0\omega^n \cos\left(\frac{n\pi}{2}\right) + jY_0\omega^n \sin\left(\frac{n\pi}{2}\right)} \quad (3)$$

Where Y_0 is the CPE coefficient and $n=1$ represents the homogeneous electrode surface. To extract the values of electrical components associated with different phenomenon, the obtained experimental Nyquist spectra in the frequency range of 100 kHz to 0.1 Hz is fitted through above discussed circuit by using MATLAB/Simulink. The fitting is optimized through multiple trials to ensure an accurate and reproducible result with a mean error of modulus <5%. In contrast to the previous reports on EIS of PANI where a vertical line is observed in the low frequency region, in the present study, the real part resistance decreases with decreasing frequency and then again increases with the decreasing frequency. The observed trend is consistent with a previous report by Žic et al.[31,42] where the author have explained this phenomenon is due to the lower value of ionic charge transfer resistance in the PANI layer (R_d). The lower value of R_d in parallel to Q_i facilitates the counter ion flux inside the PANI layer which results in a higher population of quinoidal groups inside PANI.

The dependence of EIS spectra on the applied potential (ESI†) for PANI electrodes is well explained by Hu et al. as following[43,44]: (i) the high frequency arc, independent of applied potential at potentials negative to 0.1 V is attributed to the insulating property of PANI and double layer charging and discharging process. (ii) the low frequency region, dependent on applied potential indicates the Faradaic process of bulk redox transitions of the polymer. This phenomenon is different from the case of metal electrodes and is attributed to the higher

conductivity, the charged polymer|electrolyte interface and the more reversible redox characteristics of PANI at more positive potentials. Fig. 6 depicts the Nyquist plot of PANI (H_2SO_4), PANI (H_2SO_4+$CuSO_4$) and Cu-PANI (H_2SO_4) at OCP. The value of R_s for all the three configuration is obtained in the order of PANI (H_2SO_4) > PANI (H_2SO_4+$CuSO_4$) > Cu-PANI (H_2SO_4). The series resistance R_s at electrode-electrolyte interface is ascribed to two major aspects: (i) electronic, which is related to the intrinsic electrical resistance of PANI, intrinsic resistance of current collector and the contact resistance between current collector and PANI and (ii) ionic, which is associated with the resistance of electrolyte in the inferior of PANI matrix and bulk electrolyte.

The important features of CV in Fig. 2 that influences the supercapacitor performance can also be explained on the basis of EIS fitting parameters. The physisorption of the electrolyte ion on the electrode surface can be well explained based on the values of C_{dl} and R_F. At higher frequency, the value of C_{dl} arises from the charge present at electrode surface that overcome the energy to migrate with the alternating potential.[45] The fitted value of C_{dl} obtained for PANI (H_2SO_4), PANI (H_2SO_4+$CuSO_4$) and Cu-PANI (H_2SO_4) are 7, 6.2, 22 $\mu F/cm^2$ respectively. The higher value of C_{dl} obtained for Cu-PANI (H_2SO_4) is associated with the doping of Cu into PANI which modified the PANI surface that provides a higher surface area with more accessible sites for the mobile charges near the electrode surface. While a lowest value of C_{dl} is obtained for PANI in redox additive electrolyte. This observation is corroborated by further viewing PANI morphology (Fig. 1E). The growth of Cu fractals on the PANI nanorod restricts the H^+ ion diffusion in the polymer matrix that results in supressed Faradaic reaction and charge transfer at PANI electrolyte interface. The Faradaic leakage resistance R_F represents the resistance of leakage due to overcharge or Faradaic redox reaction caused by impurities or electrode functional groups.[46] The value of R_F obtained for Cu-PANI (H_2SO_4), PANI (H_2SO_4) and PANI (H_2SO_4+$CuSO_4$) are 1.3, 1.7

and 3.1 Ω/cm^2 respectively. A lower value of R_F obtained for Cu-PANI (H_2SO_4) signifies a greater kinetic reversibility of the Faradaic reaction and lower charge accumulation at electrode-electrolyte interface. The 45° segment, during the transition from high frequency semicircle to mid frequency spike, is known as Warburg element in the Nyquist plot (Fig. 6). The length of this segment and exponent (m) indicates the resistance faced by the ion during their transport into the pores and electrode porosity, respectively.[45] From Fig. 6, PANI (H_2SO_4+$CuSO_4$) demonstrates that the highest resistance is faced by the ion during their transport in the polymer matrix, followed by PANI (H_2SO_4), with Cu-PANI (H_2SO_4) possessing the lowest resistance. The value of exponent is observed as m = 0.55 for PANI (H_2SO_4), m = 0.74 for PANI (H_2SO_4+$CuSO_4$) and m = 0.49 for Cu PANI (H_2SO_4). The lower value of exponent (m) signifies that the ion diffusion takes place at both the planar surface and inside the pores whereas a higher value of m for PANI (H_2SO_4+$CuSO_4$) indicates that only surface phenomena are associated.

The high retention of capacitance under fast charge discharge conditions is only possible if the system assists very fast ion diffusion in response to the large perturbation and possesses very low Faradaic leakage resistance R_F. Therefore the high rate retention for Cu-PANI (H_2SO_4) than the other two configurations is the direct consequence of lower R_F and lower Warburg length. It is interesting to note from the Nyquist plot of Fig. 6, that the redox additive electrolyte and doping shifts the transition frequency (the frequency at which high frequency circle changes to mid frequency spike) which is 1.47, 1 and 1.78 Hz for PANI (H_2SO_4), PANI (H_2SO_4+$CuSO_4$) and Cu-PANI (H_2SO_4) respectively. This observation suggests that there is time dependence in the discharge process on electrode and electrolyte configuration. At a very low frequency the diffusion resistance (R_d) is obtained as 50, 32 and 85 kΩ for PANI (H_2SO_4), PANI (H_2SO_4+$CuSO_4$) and Cu-PANI (H_2SO_4) respectively. The lower value of diffusion resistance implies a higher leakage current which causes the

supercapacitor to self-discharge at a faster rate. A similar conclusion for PANI in H_2SO_4+$CuSO_4$ electrolyte is drawn from the analysis of CV. The extracted values of interfacial capacitance are 0.238, 0.359 and 0.51 F/cm^2 for PANI (H_2SO_4), PANI (H_2SO_4+$CuSO_4$) and Cu-PANI (H_2SO_4) respectively. The obtained value of interfacial capacitance is comparable to the value obtained from CVs measured at 5mV/s showing the validity of fitting parameters.

Complex Frequency Analysis. Complex frequency analysis has emerged as an excellent technique for the investigation of bulk and interfacial electrochemical phenomenon, pseudo and electric double layer capacitance at low frequency.[47] Fig. 7 shows the relation between phase with the change in frequency. The phase angle changes from 73° to 82° in the order of PANI (H_2SO_4) > PANI (H_2SO_4+$CuSO_4$) > Cu-PANI (H_2SO_4).

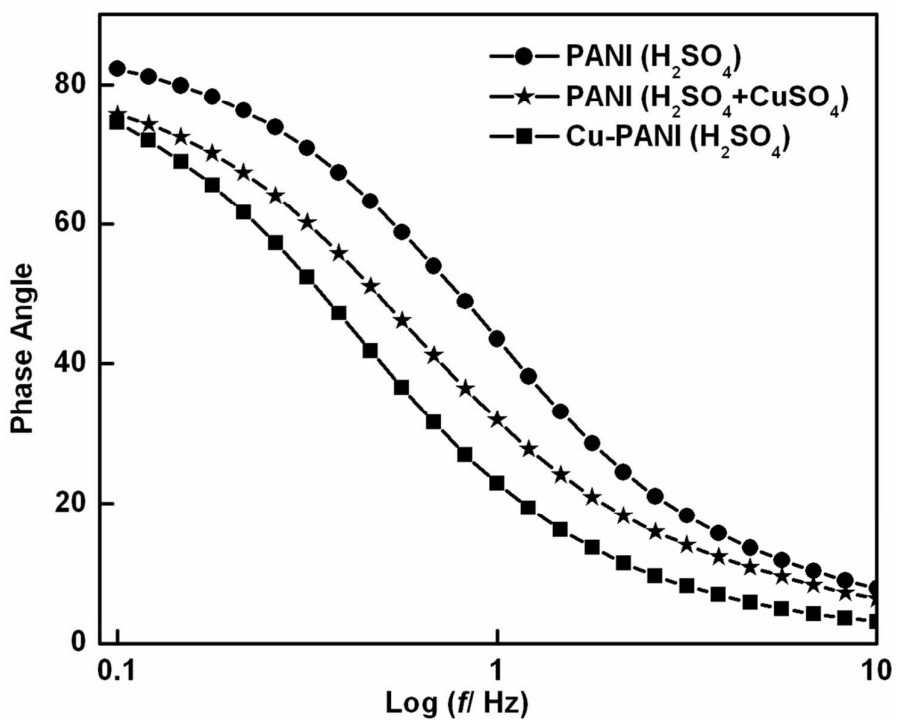

Fig. 7 Bode plot of the different configurations

The lower phase angle signifies the higher resistance and pseudo capacitive behaviour. Thus, it further confirms the outcome of CV and EIS analysis that doping of PANI with Cu offers a comparatively higher intrinsic resistance (i.e. Diffusion resistance) with a larger pseudo capacitive nature of electrode during the electrochemical process. Fig. 8 shows the real part of complex capacitance derived from the impedance spectra (Fig. 6) according to Eq. (2) for PANI (H_2SO_4), PANI (H_2SO_4+$CuSO_4$) and Cu-PANI (H_2SO_4) as a function of frequency.

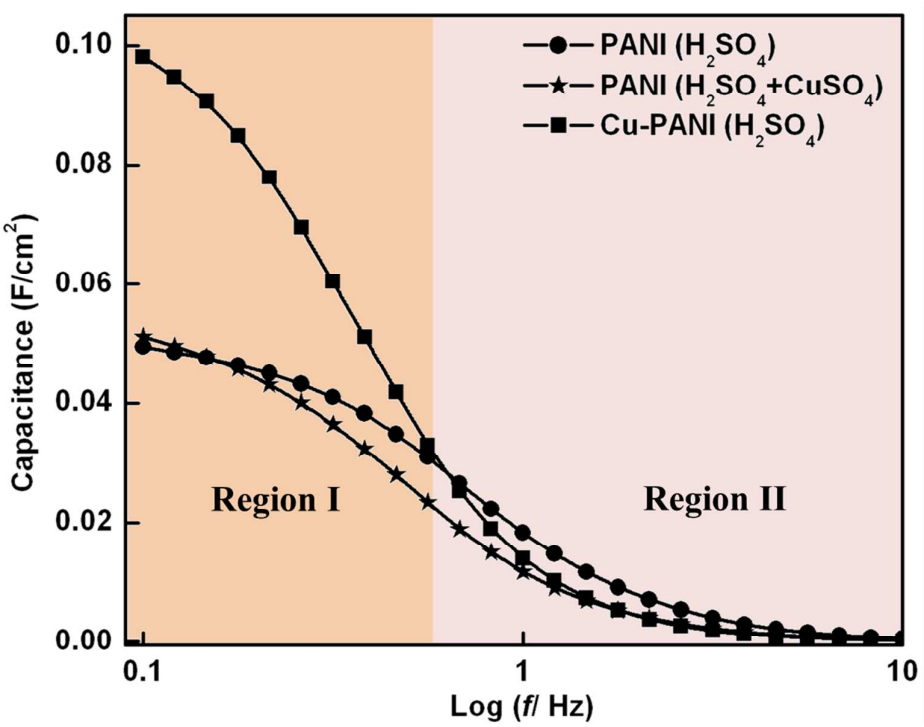

Fig. 8 Real part of complex capacitance vs. frequency for different configurations

From the plot of *C'* vs. frequency it is observed that the electrode reaches to a full capacitance at low frequency and becomes constant at a higher frequency. The obtained *C'* vs. frequency plot for all configuration are analysed in two frequency regions, i.e. region 1 (0.1 to 0.9 Hz) and region 2 (0.9 to 10 Hz). In Region I (i.e. low power and high energy), the maximum and minimum capacitance is obtained for Cu-PANI (H_2SO_4) and PANI (H_2SO_4) respectively. Whereas in Region II (i.e. high power and low energy), the maximum and

minimum capacitance is obtained for PANI (H_2SO_4) and PANI (H_2SO_4+$CuSO_4$) respectively. A dynamic change in the maximum value of capacitance between Cu-PANI (H_2SO_4) and PANI (H_2SO_4) during the transition from Region I to II is further explained by simulating the behaviour of *C'* vs. frequency.[48,49] A detailed derivation and the simulation results are shown in ESI†. From the simulation results discussed in ESI†, it is concluded that during the electropolymerization process, Cu doped PANI results in a higher polymerization rate which induces thicker electrode with higher capacitance in the low frequency region. While the non-uniform utilization of electrode current at higher frequency, causes a decrease in the value of capacitance for Cu-PANI electrode.

CONCLUSION

The role of copper (Cu) as a redox additive and dopant on the performance of PANI based supercapacitor was thoroughly investigated. The analysis of CV reveals that Cu-PANI (H_2SO_4) exhibits a comparatively higher pseudo capacitance. Whereas physisorption of PANI surface in H_2SO_4+$CuSO_4$ (redox additive) electrolyte reveals a higher pseudo capacitance with low capacity retention as compared to PANI (H_2SO_4). The capacitance of PANI (H_2SO_4+$CuSO_4$) appears to be unstable because of underpotential deposition of copper over PANI surface and its relatively irreversible redox reaction. However, a stable and improved performance was obtained for Cu doped PANI due to the combined effect of an increase in conductivity and the surface modification of PANI film. For Cu doped PANI, nearly ~2.4 and ~1.5 fold improved interfacial capacitance was achieved than that of PANI (H_2SO_4) and PANI (H_2SO_4+$CuSO_4$) respectively. The high rate retention for Cu-PANI (H_2SO_4) than the other two configurations is the direct consequence of lower R_F and lower Warburg length. The lower value of diffusion resistance for PANI (H_2SO_4+$CuSO_4$) implies a higher leakage current which causes the supercapacitor to self-discharge at a faster rate. From the simulated capacitance vs. frequency plot, it can be inferred that Cu doped PANI results in a higher

polymerization rate which induces thicker electrode with higher capacitance in the low frequency region. While the non-uniform utilization of electrode current at higher frequency, causes a decrease in the value of capacitance for Cu-PANI electrode. The present analysis thus shows the importance of understanding the role of doping and redox additive on the performance of PANI based supercapacitor and also lay the basis to design a supercapacitor with appropriate electrode and electrolyte material for numerous industrial and consumer applications.

AUTHOR INFORMATION

Corresponding Author

School of Solar Energy, Pandit Deendayal Petroleum University, Gandhinagar- 382007, Gujarat, India

Tel.: +91 – 9586864936, Fax. +91-79-23275030

E-mail address: indrajit.m@sse.pdpu.ac.in (Indrajit Mukhopadhyay)

ACKNOWLEDGEMENT

The authors gratefully acknowledge DST (Project No. SR/S1/PC-44/2011 dated 04/07/2012) for the financial assistance. One of the author (K.P.) thanks DST INSPIRE fellowship program for junior research fellowship. Ms. Purvi Kikani, FCIPT, IPR, Gandhinagar and Dr. B. P. Singh, CSIR-IMMT, Bhubaneswar is greatly acknowledged for FTIR, and Raman and XPS measurements respectively. The authors are deeply grateful to anonymous referees for their invaluable suggestions to improve the quality of this article.

REFERENCES

1. L. F. Chen, X. D. Zhang, H. W. Liang, M. Kong, Q. F. Guan, P. Chen, Z. Y. Wu and S. H. Yu, *ACS Nano,* 2012, **6**, 7092.
2. S. B. Kulkarni, U. M. Patil, I. Shackery, J. S. Sohn, S. Lee, B. Park and S. Jun, *J. Mater. Chem. A,* 2014, **2**, 4989.
3. C. Peng, D. Hu and G. Z. Chen, *Chem. Commun.*, 2011, **47**, 4105.
4. H. Fan, H. Wang, N. Zhao, X. Zhang and J. Xu, *J. Mater. Chem.*, 2012, **22**, 2774.
5. J. P. Zheng and T. R. Jow, *J. Electrochem. Soc.,* 1995, **142**, L6.
6. H. Y. Lee and J.B. Goodenough*, J. Solid State Chem.,* 1999, **148**, 81.
7. M. Rose, Y. Korenblit, E. Kockrick, L. Borchardt, M. Oschatz, S. Kaskel and G. Yushin, *Small*, 2011, **7**, 1108.
8. K. Pandey, P. Yadav and I. Mukhopadhyay, *J. Phys. Chem. B,* 2014, **118***,* 3235.
9. D. Bhattacharjya and I. Mukhopadhyay, *Langmuir,* 2012, **28**, 5893.
10. W. Chen, R. B. Rakhi and H. N. Alshareef, *J. Mater. Chem. A,* 2013, **1**, 3315.
11. W. K. Maser, A. M. Benito, M. A. Callejas, T. Seeger, M. T. Martínez, J. Schreiber, J. Muszynski, O. Chauvet, Z. Osváth, A. A. Koós, L.P. Biró, *Mater. Sci. Eng. C*, 2003, **23**, 87.
12. Z. Tai, X. Yan and Q. Xue, *J. Electrochem. Soc.*, 2012, **159**, A1702.
13. H. Mi, X. Zhang, S. Yang, X. Ye and J. Luo, *Mater. Chem. Phys.,* 2008, **112**, 127.
14. C. Meng, C. Liu and S. Fan, *Electrochem. Comm.,* 2009, **11**, 186.
15. C. C. Hu and C. H. Chu, *Mat. Chem. Phys.*, 2000, **65**, 329.
16. C. C. Hu, E. Chen and J. Y. Lin, *Electrochim. Acta*, 2002, **47**, 2741.
17. M. M. Rahman Khan, Y. K. Wee and W. A. Kamil Mahmood, *Synth. Met.*, 2012, **162**, 1065.
18. H. Xu, J. Zhang, Y. Chen, H. Lu and J. Zhuang, *RSC Adv.*, 2014, **4**, 5547.

19. S. Dhibar, S. Sahoo, C. K. Das and R. Singh, *J. Mater. Sci.: Mater. Electron.*, 2013, **24**, 576.

20. Q. Li, Kaixi Li, C. Sun and Y. Li, *J. Electroanal. Chem.*, 2007, **611**, 43.

21. L. Qian, X. Tian, L. Yang, H. Yuan and D. Xiao, *RSC Adv.*, 2013, **3**, 1703.

22. W. Chen, R. B. Rakhi and H. N. Alshareef, *Nanoscale*, 2013, **5**, 4134.

23. N. Devillers, S. Jemei, M. C. Péra, D. Bienaimé and F. Gustin, *J. Power Sources*, 2014, **246**, 596.

24. L. Li, Z. Y. Qin, X. Liang, Q. Q. Fan, Y. Q. Lu, W. H. Wu and M. F. Zhu, *J. Phys. Chem. C*, 2009, **113**, 5502.

25. S. Sharma, C. Nirkhe, S. Pethkar and A. A. Athawale, *Sens. Actuators B*, 2002, **85**, 131.

26. C. M. S. Izumi, A. M. D. C. Ferreira, V. R. L. Constantino and M. L. A. Temperini, *Macromolecules*, 2007, **40**, 3204.

27. W. C. Chen, T. C. Wen and A. Gopalan, *Synth. Met.,* 2002, **128**, 179.

28. S. Tao, B. Hong and Z. Kerong, *Spectrochim. Acta Part A*, 2007, **66**, 1364.

29. C. C. Hu and J. Y. Lin, *Electrochim. Acta*, 2002, **47**, 4055.

30. P. J. Hung, K. H. Chang, Y. F. Lee, C. C. Hu and K. M. Lin, *Electrochim. Acta*, 2010, **55**, 6015.

31. M. Žic, *J. Electroanal. Chem.*, 2007, **610**, 57.

32. J. Zheng, S. S. Moganty, P. C. Goonetilleke, R. E. Baltus and D. Roy, *J. Phys. Chem. C*, 2011, **115**, 7527.

33. H. Xie, Y. Zhu, Y. Wu, Z. Wu and E. Liu, *Mat. Res. Bull.*, 2014, **50**, 303.

34. S. T. Senthilkumar, R. Kalai Selvan and J. S. Melo, *J. Mater. Chem. A*, 2013, **1**, 12386.

35. W. Gu, M. Sevilla, A. Magasinski, A. B. Fuertes and G. Yushin, *Energy Environ. Sci.*, 2013, **6**, 2465.

36. G. Sun, K. Li and C. Sun, *Microporous Mesoporous Mater.*, 2010, **128**, 56.

37. C. K. Wu, M. Yin, S. O'Brien and J. T. Koberstein, *Chem. Mater.*, 2006, **18**, 6054.

38. N. G. Skinner and E. A. H. Hall, *Synth. Met.,* 1994, **63**, 133.

39. C. C. Hu, J. C. Chen and K. H. Chang, *J. Power Sources,* 2013, **221**, 128.

40. K. Pandey, P. Yadav and I. Mukhopadhyay, *J. Solid State Electrochem.*, 2014, **18**, 453.

41. P. Yadav, B. Tripathi, K. Pandey and M. Kumar, *Phys. Chem. Chem. Phys.*, 2014, DOI: 10.1039/C4CP01115E.

42. M. Žic, *J. Electroanal. Chem.*, 2009, **635**, 29.

43. C. C. Hu and C. H. Chu, *J. Electroanal. Chem.*, 2001,**503**, 105.

44. W. C. Chen, T. C. Wen, C. C. Hu and A. Gopalan, *Electrochim. Acta*, 2002, **47**, 1305.

45. C. Masarapu , H. F. Zeng , K. H. Hung and B. Wei, *ACS Nano*, 2009, **3**, 2199.

46. M. Kotal, A. K. Thakur and A. K. Bhowmick, *ACS Appl. Mater. Interfaces*, 2013, **5**, 8374.

47. C. Yang, M. Zhou and Q. Xu, *Phys. Chem. Chem. Phys.*, 2013, **15**, 19730.

48. V. Srinivasan and J. W. Weidner, *J. Electrochem. Soc.*, 1999, **146,** 1650.

49. S. Motupally, C. C. Streinz and J. W. Weidner, *J. Electrochem. Soc.*, 1995, **142**, 1401.

Graphical Abstract

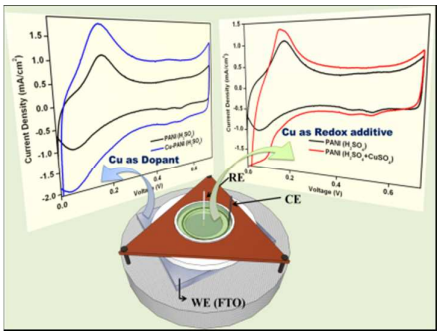

Role of transition metal as a dopant or redox additive essential for designing high power/ high energy supercapacitor is investigated.